Master's Thesis

Calculation of Vertical Flux and Diffusivity due to Double Diffusion in the Tropical Western Pacific

적도 서태평양에서 이중 확산에 의한
수직 혼합 산출

August 2014

The Graduate School of Seoul National University

School of Earth and Environmental Sciences

Chorong Lee

Calculation of Vertical Flux and Diffusivity due to Double Diffusion in the Tropical Western Pacific

A dissertation submitted in partial fulfillment of the requirements for the degree of Master of Science in the School of Earth and Environmental Sciences/Graduate School of Seoul National University

by

Chorong Lee

June 2014

We accept this dissertation as conforming to the required standard.

Chair Kwang-Yul Kim (인)

Vice Chair Kyung-Il Chang (인)

Examiner Jae Hak Lee (인)

Professor Kwang-Yul Kim, Chair/Departmental Member (Seoul National University)

Professor Kyung-Il Chang, Vice-chair/Supervisor (Seoul National University)

Dr. Jae Hak Lee, External Examiner (Korea Institute of Ocean Science and Technology)

Abstract

This study aims to understand the impacts of double diffusion and turbulence on vertical mixing in thermocline (from 20 m to below 300 m depth) under weak turbulence condition based on 14-day time series observation of fine scale velocity and temperature at 0˚ N, 156˚ E in 2012. The observation allows direct estimates of temperature variance dissipation rate and turbulent kinetic energy dissipation rate. The weak turbulence condition appears to the result from the restricted vertical turbulent mixing due to westward expansion of fresher warm pool which was reported to occur in the western equatorial Pacific during the El Nino period. Vertical diffusivity and vertical flux of heat, salt, and density are calculated using the methods from *McDougall and Ruddick* [1992]. The Turner angle and the Reynolds number are used to classify observed regimes into neither turbulent nor double diffusive, turbulent, non-turbulent double diffusive, and turbulent double diffusive regimes. The results suggest a considerable contribution of double diffusion to vertical flux of heat and salt larger than that due to turbulence by a factor of 10 – 100. The magnitude of vertical flux of temperature and salinity due to salt fingering is estimated to be about 10^{-6} – 10^{-7} K m s^{-1} and 10^{-5} – 10^{-6} psu m s^{-1}. The dominance of the double diffusive vertical flux results in downward total density flux of about 10^{-7} kg m^{-2} s^{-1} rather than upward flux which is the case for the turbulence-dominated vertical flux. Vertical density diffusivity due to double diffusion

is 10^{-5} – 10^{-7} m^2 s^{-1}, which is comparable with that due to turbulence in 10 times greater turbulent dissipation condition. This study highlights the substantial contribution of double diffusion to vertical density flux in the tropical western Pacific under weak turbulence condition. Estimates of the vertical flux based only on turbulence would significantly underestimate the vertical density flux.

Keywords: Turbulence, Double diffusion, Vertical mixing, Tropical western Pacific
Student Number: 2012-23080

CONTENTS

List of Table

List of Figure

Chapter 1. Introduction

In the western equatorial Pacific, strong meridional gradients of temperature and salinity persist due to the convergence of warm and salty South Pacific and cool and fresher North Pacific waters. In this region, double diffusion is thought to be a cause of observed interleaving features [*Richards and Banks*, 2002; *Richards and Pollard*, 1991; *Ruddick and Richards*, 2003]. Two major westward currents are South Equatorial Current (SEC) at the surface and Equatorial Intermediate Current (EIC) reaching much deeper than thermocline. Both are very weak in the western equatorial Pacific. Strong eastward Equatorial Undercurrent (EUC) driven by shoaling thermocline exists between the SEC and the EIC [*Johnson*, 2002; *Tomczak and Godfrey*, 2003].

Much work has been done on vertical mixing in surface and thermocline of the tropical Pacific, especially in the eastern Pacific. Deep-reaching diurnal cycle of surface turbulent mixing caused by surface heat flux and wind is common feature of upper ocean [*Gregg et al.*, 1985; *Moum and Caldwell*, 1985; *Moum et al.*, 1989]. In the subsurface of eastern equatorial Pacific, the shear of EUC and Tropical Instability Wave enhance mechanical mixing [*Gregg et al.*, 1985; *Moum et al.*, 2009, 2013]. Small-vertical-scale Velocity Structures (SVSs) of unknown origin are reported to be important in vertical mixing in the western equatorial Pacific [*Richards et al.*, 2012].

The relationship between vertical mixing and El Niño Southern Oscillation (ENSO) also attracted the attention of scientists. In the western equatorial Pacific, upper ocean states are dependent on ENSO cycle; warm pool expands toward east concurrent with the strengthening of surface eastward flow due to weakening of trade wind during El Niño periods [*Johnson et al.*, 2002; *Maes et al.*, 2006]. This gives rise to an enhanced stratification and weakening of turbulent vertical mixing [*Richards et al.*, 2012]. In a coupled general circulation model (CGCM), the amplitude of ENSO is dependent on vertical diffusivity [*Meehl et al.*, 2001]. *Sasaki et al.* [2013] showed that background diffusivity considering SVSs improves the performance of ENSO simulation in CGCM.

On the contrary, little research has been carried out on how double diffusive mixing varies as ocean state and turbulent mixing change. Turbulence break sharp diffusive interface across which heat and salt are transported efficiently [*Linden*, 1971]. Observed turbulent level at this interface is sufficiently weak [*Gregg*, 1988; *Padman and Dillon*, 1987]. Therefore, double diffusion can be active in this region when turbulence is weak enough not to disturb its interface.

In this study, we examine the effect of double diffusion on vertical mixing and the connection with thermohaline structure related with stratification based on micro-scale data acquired during MIXing in Equatorial Thermocline (MIXET) cruise to investigate turbulent mixing due to SVSs. Field observations and data processing are explained in chapter 2. In the same chapter, we introduce

calculation methods of vertical flux and diffusivity using observed data in four different regimes; none, turbulence, non-turbulent double diffusion, turbulent double diffusion. The results of vertical flux and diffusivity due to double diffusion are shown in chapter 3. The analysis how they relate with ocean state and regimes is followed.

Chapter 2. Data and Method

1. Observation

Conductivity-Temperature-Depth (CTD, SBE 911plus) data, Lowered Acoustic Doppler Current Profiler (LADCP, 600 kHz) data, and microstructure data using the Turbulence ocean Microstructure Acquisition Profiler (TurboMAP) were acquired during MIXET second cruise between 25th Oct. 2012 and 18th Nov. 2012 in collaboration with University of Hawaii (UH). Time series measurement was conducted at 0° N and 156° E for 14 days, and a meridional section was occupied twice along 156° E before and after the time series measurement. The first section took place from 5º N to 2º S at every 0.5º interval followed by the time-series measurement every 3-hr. The second section was occupied with two different spatial intervals; every 0.125º interval from 0.5º S to 0.5º N to obtain detailed meridonal structures around equator, and 1.5º N, 3.2º N, 4.5º N (Figure 1). CTD and LADCP were lowered down to 400 m to observe thermohaline structure and velocity fields. Fine-scale profiles of velocity and temperature in the upper 300 m are measured with TurboMAP during the time series observation to estimate the dissipation rate of turbulent kinetic energy per unit mass (ε) and the rate of loss of temperature variance (χ).

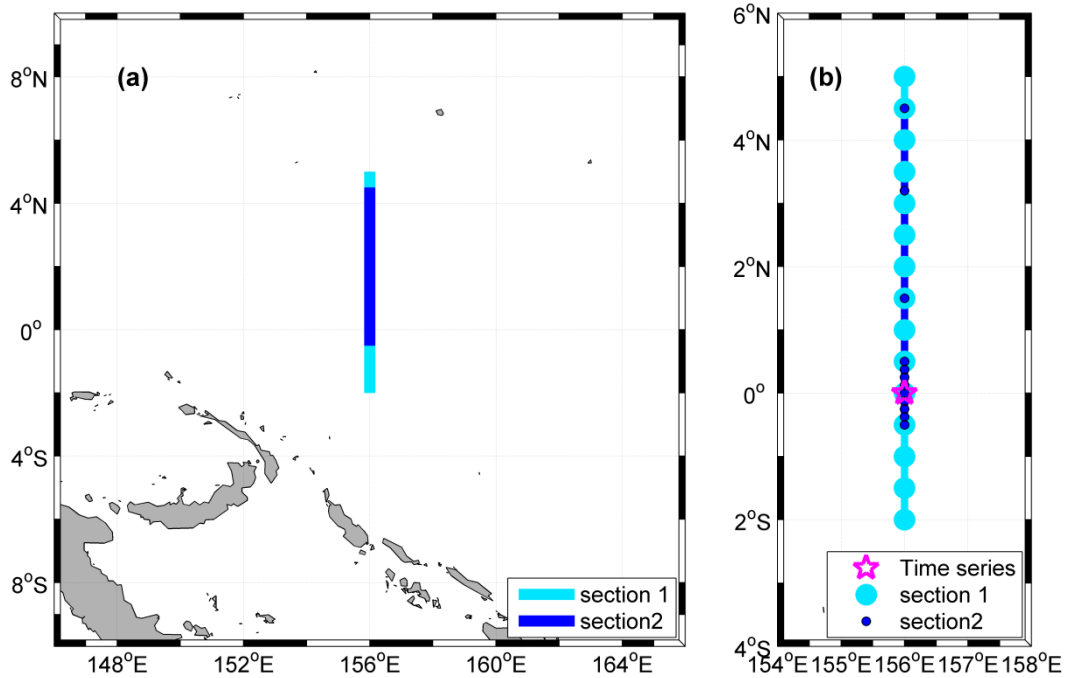

Figure 1. (a) Observed 156º E lines, (b) Detailed station map. Light blue line is section 1 and blue line is section 2. Magenta star is the location doing time series.

2. Glossary of Symbols

Superscript turb = values due to turbulence

Superscript dd = values due to double diffusion

Superscript obs = observed values

Subscript z = vertical gradient of values (upward)

$\bar{}$	Temporal averaging variable which is projected onto stretched depth
T'	$T' = T(t) - \bar{T}$, perturbation temperature (°C)
$\bar{\theta}$	Temporal mean potential temperature (°C)
$\overline{\theta_z}$	Temporal mean vertical gradient of potential temperature (°C m^{-1})
θ'	$\theta' = \theta(t) - \bar{\theta}$, perturbation potential temperature (°C)
$\bar{S}$	Temporal mean salinity (psu)
$\bar{S}_z$	Temporal mean vertical gradient of salinity (psu m^{-1})
$\bar{\rho}$	Temporal mean potential density (kg m^{-3})
$\overline{\rho_z}$	Temporal mean potential density (kg m^{-4})
ρ'	$\rho' = \rho(t) - \bar{\rho}$, perturbation potential density (kg m^{-3})
$\overline{U}$	Temporal mean velocity vector (m s^{-1})
U'	$U' = U(t) - \overline{U}$, perturbation velocity vector (m s^{-1})
$\overline{u_z}$	Temporal mean vertical gradient of zonal velocity (s^{-1})
$\overline{v_z}$	Temporal mean vertical gradient of meridional velocity (s^{-1})
w	Vertical velocity (m s^{-1})
w'	$w' = w(t) - \overline{w}$, perturbation vertical velocity (m s^{-1})

g Gravity acceleration (m s^{-2})

N^2 $N^2 = g(\alpha\overline{\theta_z} - \beta\overline{S_z})$, square of buoyancy frequency (s^{-2})

S^2 $S^2 = \overline{u_z}^2 + \overline{v_z}^2$, squared shear of temporal mean horizontal velocity (s^{-2})

Γ Mixing efficiency, the ratio of potential energy gain to turbulent kinetic energy dissipation

α Thermal expansion coefficient (K^{-1})

β Saline contraction coefficient (psu^{-1})

γ $\gamma = \alpha F_\theta / \beta F_S$, density flux ratio, the ratio of the flux of density associated with heat to that of salt

ε $\varepsilon = 15\nu/2\langle(u_z)^2\rangle$, the rate of dissipation of turbulent kinetic energy, $\langle\ \rangle$ denotes spatial averaging ($m^2\ s^{-3}$)

ν Molecular kinematic viscosity ($m^2\ s^{-1}$)

χ $\chi = 6\kappa_T\langle(T'_z)^2\rangle$, the rate of loss of temperature variance ($K^2\ s^{-1}$)

κ_T Molecular thermal diffusivity ($m^2\ s^{-1}$)

J_b $J_b = -g\overline{\rho' w'}/\bar{\rho}$, buoyancy flux ($m^2\ s^{-3}$)

Re $Re = \varepsilon/(\nu N^2)$, buoyancy Reynolds number, the intensity of turbulence relative to the turbulence-suppressing effect of stability and viscosity

R_f $R_f = (-g\overline{\rho' w'}/\bar{\rho})/\left(\overline{U' w'} \cdot \overline{U}_z\right)$, flux Richardson number, the ratio of potential energy gain to the turbulent kinetic energy input by the velocity shear

R_ρ $R_\rho = \alpha\overline{\theta_z}/\beta\overline{S_z}$, density ratio, the ratio of stratification due to salt to that due to heat

Tu $Tu = \arctan(\alpha\overline{\theta_z} - \beta\overline{S_z}, \alpha\overline{\theta_z} + \beta\overline{S_z})$, Turner angle, a parameter used to define the local stability of an inviscid water column to double- diffusive convection (º)

3. Processing Data

Processed CTD and LADCP data were provided by UH. Temperature and salinity profiles from CTD were bin averaged at every 1 m interval. Horizontal velocity profiles from LADCP were obtained every 2 m in the vertical. TurboMAP also carries slow-response temperature and salinity sensors, but we use CTD profiles for following calculations because data processing using SBE software is more accurate. During the time series observation, CTD and LADCP package was first lowered and recovered. Right after the recovery of the package, TurboMAP was lowered. Hence, there is about 30-minutes gap between the CTD/LADCP data and micro-profile data from Turbo MAP.

TurboMAP has two shear probes to measure velocity shear directly. Assuming the isotropic condition, profiles of ε are calculated from the vertical shear of one velocity component. Natural turbulent dissipation has wavenumber spectra over a range of length scales and usually peaks at length scales 5-10 times larger than the Kolmogorov length scale (l_K), at which viscous dissipation becomes significant converting turbulent kinetic energy into heat energy [*Thorpe*, 2005]. Only about 13% of the turbulent energy is contained in the wavelength range greater than 5 l_K [*Wolk et al.*, 2002]. Because the length scale of the TurboMAP probes, 10^{-4} m, is too large to calculate ε integrating velocity shear profiles directly, the spectra of

the velocity shear are fitted to a known spectrum, 'Nasmyth Universal Spectrum' [*Nasmyth*, 1973]. Similarly, χ is estimated from fine-scale vertical fluctuations of temperature. Its spectra are also fitted to 'Batchelor Universal Spectrum' [*Batchelor*, 1959].

Spectral analysis was performed using 'TMtools', data processing and analysis software for TurboMAP provide by its manufacture. To give sufficient depth range for fitting, ε and χ are estimated at every 2 m and 4 m depth ranges, overlapping 2 m to secure enough depth range for spectral analysis. We also calculate ε using a software (GC soft) provided by Prof. Glenn Carter at UH. Figure 2 shows 14-day mean ε profiles from two softwares. In Figure 2, ε exceeding 10^{-7} m^2 s^{-3} are not shown. The low values of ε over 150 – 250 m from GC soft are smaller than those from TMtools. In other depth range, ε have nearly same values. This can be caused by the different setting of base level. Because the noise level of ε by TurboMAP is $3\text{-}5\times10^{-10}$ m^2 s^{-3}, TMtools tend not to provide ε lower than this value. In the case of GC soft, it calculate ε by computing l_K. For a consistency with previous researches in UH, ε calculated from GC soft is used in this study.

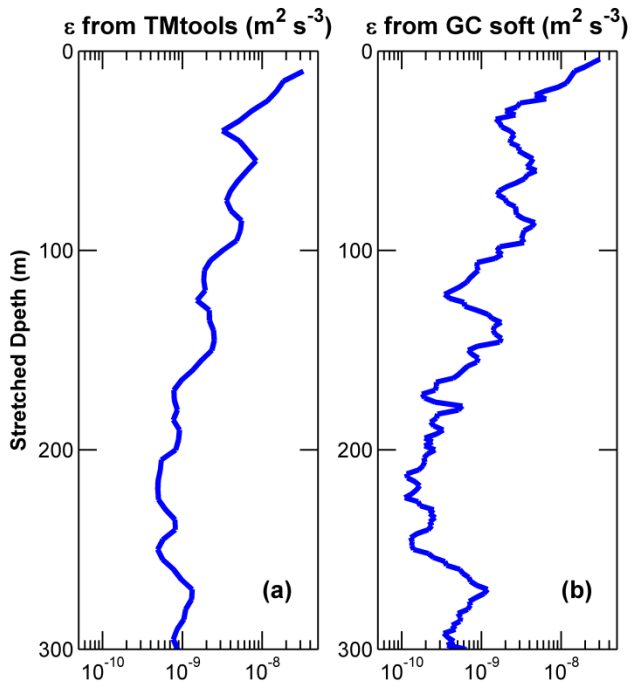

Figure 2. Vertical profiles of ε (a) from TMtools, (b) from GC soft.

4. Criteria for Turbulent and Double Diffusive Regimes

Previous studies suggest that the vertical mixing due to turbulence is effective in stratified ocean when Re exceeds 19–25 [*Gregg*, 1988; *Inoue et al.*, 2007; *Itsweire et al.*, 1993; *Padman and Dillon*, 1987]. In this study, we choose 20.

For double diffusion, Tu has been used to define the stability of water column to double diffusion [*Richards and Banks*, 2002; *Thorpe*, 2005] .

① $-180 < Tu < -90,\ 90 < Tu < 180$: doubly unstable

② $45 < Tu < 90$: salt finger

③ $-90 < Tu < -45$: diffusive convection

④ $-45 < Tu < 45$: doubly stable

Therefore, the ocean condition is classified four states in Table 1.

	Reynolds number (Re)	Turner angle (Tu)
None	$Re < 20$	$-45 < Tu < 45$
Turbulence	$Re > 20$	$-45 < Tu < 45$
Non-turbulent double diffusion	$Re < 20$	$-90 < Tu < -45$ $45 < Tu < 90$
Turbulent double diffusion	$Re > 20$	$-90 < Tu < -45$ $45 < Tu < 90$

Table 1. Criteria for four cases; none, turbulence, non-turbulent double diffusion, and turbulent double diffusion (we ignore the Turner angle range that corresponds to doubly unstable.)

5. Calculation of Vertical Diffusivity and Vertical Flux of Heat, Salt, and Density

We calculate vertical diffusivity and flux of heat, salt, and density following the methods from *McDougall and Ruddick* [1992]. They derived the method for calculating the vertical flux in the presence of both salt-fingering and mechanically driven turbulent mixing based on previous studies on vertical flux due to entirely turbulence or double diffusion. Because vertical diffusivity and flux using log normally distributed ε and χ have significant uncertainty, *McDougall and Ruddick* [1992] averaged all values vertically over 100 m, thus vertical structure of diffusivity and flux are unknown. To avoid this problem, we use 14-day time series data, sufficiently longer than turbulent time scale. All data are time-averaged after projected onto stretched depth, interpolating onto potential density and then interpolated back onto the mean depth of density surfaces to remove density fluctuations [*Richards and Banks*, 2002].

5.1. Case for Turbulent Regime

When the vertical mixing is dominated by turbulence, the turbulent kinetic energy equation below for the steady state is used for calculating vertical diffusivity and vertical flux.

$$0 = -\overline{U'w'} \cdot \bar{U}_z - \varepsilon - g\frac{\overline{\rho'w'}}{\bar{\rho}} \qquad (1)$$

The three terms on the right represent 1) the rate of production of turbulent kinetic energy by the shear, 2) the rate of dissipation of kinetic energy by the turbulence, and 3) the buoyancy flux. From this equation, vertical turbulent density diffusivity is

$$K_\rho = \frac{\overline{\rho'w'}}{\bar{\rho}_z} = \left[\frac{R_f}{1-R_f}\right]\frac{\varepsilon}{N^2} = \Gamma^{turb}\frac{\varepsilon}{N^2} \qquad (2)$$

Γ^{turb} is the turbulent mixing efficiency. For strong turbulent case, 0.2 is taken [*Osborn*, 1980; *Moum*, 1996]. Generally, K_ρ has positive value of 10^{-4} m^2 s^{-1} for global averaging, 10^{-5} m^2 s^{-3} for abyssal ocean [*Kantha and Clayson*, 2000]. Corresponding upward density flux increases potential energy of water column.

Assuming the mechanical mixing due to turbulence for heat and salt is equal to that for density, vertical diffusivity and corresponding flux for the turbulent regime are

$$K_\rho = K_\theta = K_s = \Gamma^{turb}\frac{\varepsilon}{N^2} \qquad (3)$$

$$F_\rho = -K_\rho\overline{\rho_z} = -\Gamma^{turb}\frac{\varepsilon}{N^2}\overline{\rho_z} \qquad (4)$$

$$F_\theta = -K_\theta\overline{\theta_z} = -\Gamma^{turb}\frac{\varepsilon}{N^2}\overline{\theta_z} \qquad (5)$$

$$F_S = -K_S\overline{S_z} = -\Gamma^{turb}\frac{\varepsilon}{N^2}\overline{S_z} \qquad (6)$$

5.2. Case for Double Diffusive Regime

When the vertical mixing is entirely determined by non-turbulent double diffusion, there is no source term in equation (1); vertical mixing get energy from available potential energy, not from vertical shear.

$$0 = -\varepsilon - g\frac{\overline{\rho' w'}}{\bar{\rho}} \qquad (7)$$

From this equation, vertical diffusivity and corresponding flux for double diffusion can be written as

$$K_\theta = -\frac{F_\theta}{\overline{\theta_z}} = \frac{1-\frac{1}{R_\rho}}{\frac{1}{\gamma}-1}\frac{\varepsilon}{N^2} = \frac{\gamma}{R_\rho}K_S \qquad (8)$$

$$K_S = -\frac{F_S}{\overline{S_z}} = \frac{R_\rho - 1}{1-\gamma}\frac{\varepsilon}{N^2} = \frac{R_\rho}{\gamma}K_\theta \qquad (9)$$

$$K_\rho = -\frac{F_\rho}{\overline{\rho_z}} = \frac{\rho_0(\alpha F_\theta - \beta F_S)}{\bar{\rho}_z} = \frac{\varepsilon}{N^2} \qquad (10)$$

$$F_\theta = -K_\theta \overline{\theta_z} = -\frac{1-\frac{1}{R_\rho}}{\frac{1}{\gamma}-1}\frac{\varepsilon}{N^2}\overline{\theta_z} \qquad (11)$$

$$F_S = -K_S \overline{S_z} = -\frac{R_\rho - 1}{1-\gamma}\frac{\varepsilon}{N^2}\overline{S_z} \qquad (12)$$

$$F_\rho = -K_\rho \overline{\rho_z} = -\frac{\varepsilon}{N^2}\overline{\rho_z} \qquad (13)$$

Because double diffusion releases potential energy to drive the motion, F_ρ is downward and K_ρ is negative. Compare equation 3 and 10, K_ρ due to double diffusion is generally because under same condition, for double

diffusive motion is only vertical not in three dimensions like turbulence [*Kantha and Clayson*, 2000]. R_ρ is easily calculated from vertical temperature and salinity profiles, but for the calculation of γ temperature and salinity flux are required. Double diffusive instability induces vertical motion releasing potential energy [*Tomczak and Godfrey*, 2003]. The dominant buoyancy flux is salt flux for salt fingering but heat flux for diffusive convection. So, we need to calculate γ for each case without the prior knowledge of temperature and salinity fluxes.

Kunze [1987] develops a quasi-steady-state model for fastest-growing salt fingers, and expresses γ as a function of R_ρ

$$\gamma = \sqrt{R_\rho}\left(\sqrt{R_\rho} - \sqrt{R_\rho - 1}\right) \qquad (14)$$

Kelley [1990] provides an empirical curve of γ on R_ρ for diffusive convection based on published measurements.

$$\gamma = \frac{1 + 14\left(\frac{1}{R_\rho} - 1\right)^{3/2}}{\frac{1}{R_\rho} + 1.4\left(\frac{1}{R_\rho} - 1\right)^{3/2}} \qquad (15)$$

5.3. Case for Co-existence of Turbulence and Double Diffusion

When both turbulence and double diffusion are present, we assume that the observed dissipation of kinetic energy and the observed buoyancy flux

are the linear summation of those due to turbulence and double diffusion because the space and time scales of both types are quite different to interact.

$$\varepsilon^{obs} = \varepsilon^{turb} + \varepsilon^{dd} \qquad (16)$$

$$J_b^{obs} = J_b^{turb} + J_b^{dd} \qquad (17)$$

Then the equation of turbulent kinetic energy can be written as

$$\left[-\overline{U'w'} \cdot \bar{U}_z - \varepsilon^{turb} + J_b^{turb}\right] + \left[-\varepsilon^{dd} + J_b^{dd}\right] = 0 \qquad (18)$$

The former bracket is same as equation (1), and the latter as equation (7). Each bracket must be zero.

The total flux of heat and salt are caused by both turbulence and double diffusion. Because it is hard to separate each flux component from total flux, *McDougall and Ruddick* [1992] suggested the comparison of the total flux calculated from the conservation equation of potential temperature with the turbulent flux, assuming observed dissipation rate for this case is entirely due to turbulence (equation 1) [*Osborn*, 1980].

The fluctuation part of conservation equation of potential temperature is

$$\frac{\partial \theta'}{\partial \mathrm{t}} + \bar{U} \cdot \nabla\theta' + U' \cdot \nabla\theta' + U' \cdot \nabla\bar{\theta} = \nabla \cdot [\kappa_T \nabla\theta'] \qquad (19)$$

Multiplying by θ' and averaging, we obtain the equation of the temporal rate of change of thermal variance.

$$\frac{\partial \overline{\theta'^2}}{\partial \mathrm{t}} = -\nabla \cdot \left[\overline{\theta'^2}\bar{U} + \overline{U'\theta'^2} - \kappa_T \nabla\left[\overline{\theta'^2}\right]\right] - 2\overline{\theta' U'} \cdot \nabla\bar{\theta}$$

$$- 2\kappa_T \overline{\nabla\theta' \cdot \nabla\theta'} \qquad (20)$$

Terms on the right hand side represent 1) the transport divergence, 2) the production by turbulent heat flux down the mean potential temperature gradient, and 3) the dissipation by molecular diffusion. If the motion is statistically steady and homogeneous, we can neglect the temporal change and the transport divergence terms, and then the production by turbulent heat flux is balanced by the molecular dissipation. θ' from this observation is almost O(10^{-1}) °C (mean: 5.8×10^{-6} °C, standard deviation: 0.71). Then total vertical flux of potential temperature is

$$F_\theta = \overline{\theta' U'} = -\frac{\chi}{2\bar{\theta}_z} \qquad (21)$$

where the definition of χ comes from equation (20).

$$\chi = 2\kappa_T \overline{\nabla\theta' \cdot \nabla\theta'} \qquad (22)$$

The total heat flux can be also expressed in terms of mixing efficiency,

$$F_\theta = -\Gamma^{obs} \frac{\varepsilon^{obs}}{N^2} \bar{\theta}_z \qquad (23)$$

where Γ^{obs} is observed mixing efficiency, expressed as,

$$\Gamma^{obs} = \frac{F_\theta}{\bar{\theta}_z} \frac{N^2}{\varepsilon^{obs}} = \frac{\chi N^2}{2\varepsilon^{obs}(\bar{\theta}_z)^2} \qquad (24)$$

Actual calculation of Γ^{obs} using the four variables, $\chi, \varepsilon, N^2, \bar{\theta}_z$, yields large uncertainty and a wide range of values, and the variance of calculated vertical diffusivity is significantly influenced by Γ^{obs} [*Mcdougall and Ruddick*, 1992; *St. Laurent and Schmitt*, 1999]. In this study, temporal averaged data are used to calculate Γ^{obs}. χ and ε are averaged after interpolated onto stretched depth. N2 and $\bar{\theta}_z$ are calculated using

temporal averaged vertical temperature and salinity profile onto stretched depth.

As we mentioned above, assuming ε^{obs} is entirely caused by mechanical mixing, the turbulent diffusivity becomes

$$K_0 = \Gamma^{turb} \frac{\varepsilon^{obs}}{N^2} \qquad (25)$$

The ratio of total heat flux in equation (23) to turbulent heat flux using equation (25) is called 'heat flux enhancement factor' [*Mcdougall and Ruddick*, 1992]. It shows how much total heat flux is enhanced by double diffusion from turbulent heat flux.

$$\frac{F_\theta}{-K_0 \bar{\theta}_z} = \frac{\Gamma^{obs}}{\Gamma^{turb}} \qquad (26)$$

Similar approach can be applied to total salt flux by defining 'salt flux enhancement factor' [*Mcdougall and Ruddick*, 1992].

$$\frac{F_S}{-K_0 \bar{S}_z} = \frac{K_S^{turb} + K_S^{dd}}{K_0} = 1 + M_0 \left[\frac{\Gamma^{obs}}{\Gamma^{turb}} - 1 \right] \qquad (27)$$

where

$$M_0 = \frac{\left\{ \frac{R_\rho}{\gamma} \left[1 - \frac{1}{R_\rho} \right] - \Gamma^{turb} \left[\frac{1}{\gamma} - 1 \right] \right\}}{\left\{ \left[1 - \frac{1}{R_\rho} \right] - \Gamma^{turb} \left[\frac{1}{\gamma} - 1 \right] \right\}} \qquad (28)$$

Chapter 3. Results

1. Spatial and Temporal Structure of Observed Quantities

The meridional velocity field and thermohaline structure are shown in Figures 3, 4. Two strong eastward currents are the EUC centered at 200 m depth at the equator and the North Equatorial Countercurrent (NECC) in the entire 300 m depth range at 3º N. Above and below the EUC, the westward SEC and EIC can be seen (Figure 3a). S^2 has higher value at the interface between SEC and EUC. Salinity contours show a large intrusion of saline waters from south over 80 - 150 m depth with shoaling of its core on Section 2 occupied about 15 days after Section 1 (Figures 3e and 4e). In association with the intrusion, interleaving layers can also be seen. Two peak layers of N^2 are coincident with this intrusion (Figures 3f and 4f).

Figure 5 shows time series and mean profiles of velocity components and S^2. The core of SEC and EUC is clearly seen at the depth of 80 m and 200 m, respectively. Velocity shear is large around SEC core and the boundary between SEC and EUC.

The thermohaline and N^2 profiles from time series data are shown in Figure 6. Below 80 m, background temperature and salinity decrease with depth except around 200 m depth where cold and fresh water intrusions exist, so salt fingering can take place. Double diffusive interleaving is

clearly shown over 150 – 250 m and appears to propagate up and down from 200 m possibly by advection. Two peaks of buoyancy frequency are caused by salinity increase at 80 m and rapid temperature drop at 140 m.

Figure 7 shows time series and mean profile of Turner angle, ε, and χ projected onto stretched depth. During the entire observation period, vertical structure of temperature and salinity favors salt fingering below 100 m. Diffusive convection can occur above 80 m, and around 200 m and 250 m. Since these layers experienced temporal changes during the observation period (Figure 7a), we divide the entire period into three parts equally and calculate vertical flux and diffusivity in each of those three parts as well as the vertical flux and diffusivity averaged over the entire period. Time series and mean vertical profile of ε show that turbulent mixing is only dominant above 90 m. A large value of ε also appears at 140 m depth where velocity shear has the second peak. Mean profile of χ shows fluctuating features similar to the temperature gradient (Figure 8d).

The magnitude of ε below 100 m except around 140 m in this survey is about $O(10^{-10})$ m^2 s^{-3} smaller than typical smallest value of previous observations in tropical subsurface is $O(10^{-9})$ m^2 s^{-3} [*Gregg et al.*, 1985; *Lien et al.*, 1995; *Moum et al.*, 2009; *Richards et al.*, 2012; *Schmitt et al.*, 2005]. The magnitude of ε below 100 m from this observation is comparable with that in abyssal ocean [*Thorpe*, 2005] or in entirely double diffusive region [*St. Laurent and Schmitt*, 1999]. The intensity of turbulence in this region can be related with zonal velocity shear, SVSs, internal wave, and

stratification. *Richards et al.* [2012] suggest that warm and fresh water coming from the west causes strong stratification near the surface in the western equatorial Pacific under El Niño condition. It can reduce the vertical mixing due to SVSs in the thermocline region. The Southern Oscillation Index in Oct. and Nov. 2012 was 2.9 and 3.4, respectively far from El Niño or La Niña. But strong stratification at 80 m caused by relatively fresh upper ocean (Figure 6d) is similar to the ocean state during El Niño period (Figure 6). Therefore, stratification due to surface fresh water could be the main cause of changes in turbulent mixing in the thermocline in western equatorial Pacific, and the inter-annual variation of surface stratification is sometimes not related to ENSO state. Because the horizontal scales of interleaving in western equatorial Pacific are 100 km in meridional [*Richards and Pollard*, 1991; *Richards and Banks*, 2002; *Ruddick and Richards*, 2003] and excess of 700 km in zonal [Lee and Richards, 2004], time series data was observed in interleaving from the beginning to the end. Also, this turbulence change can effect on a wide area in the interfaces of double diffusive interleaving.

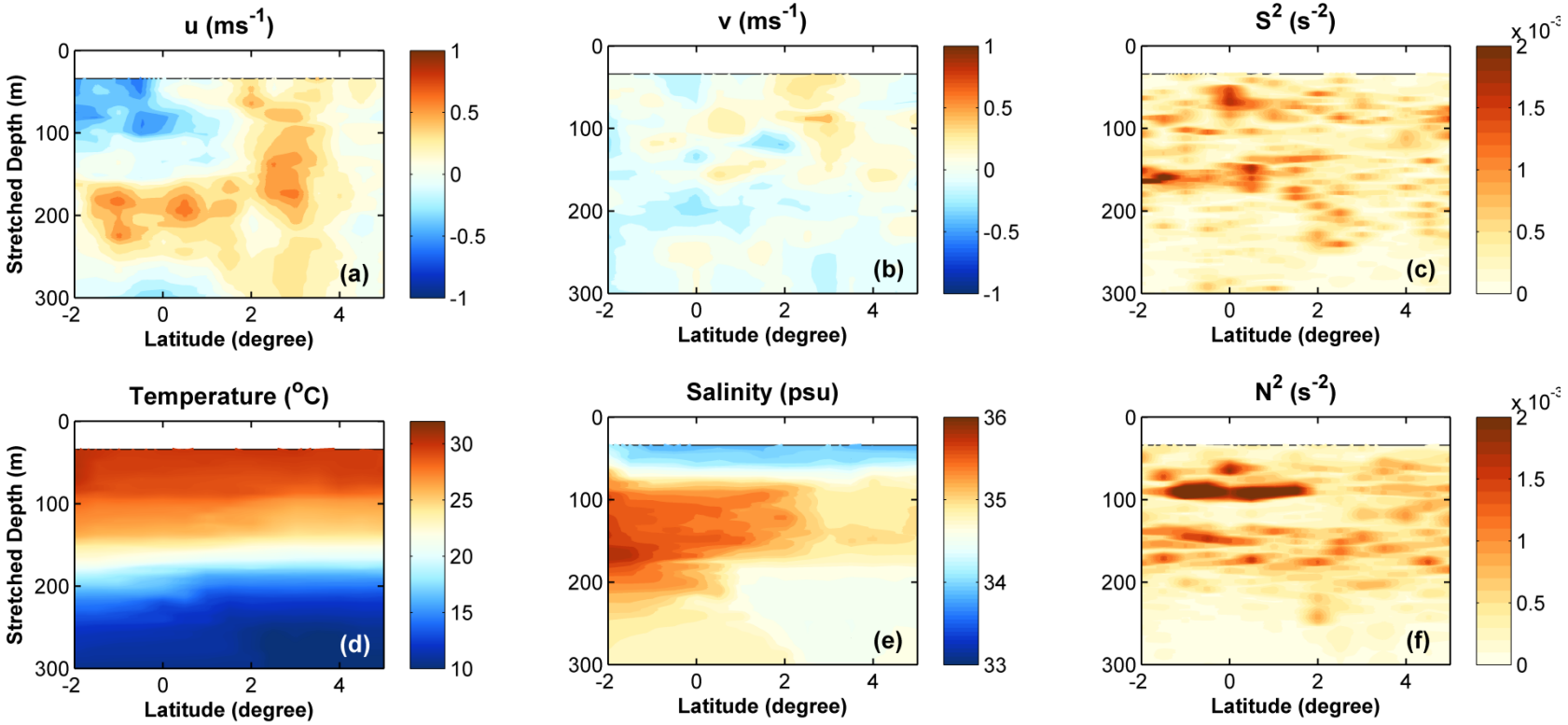

Figure 3. Section 1 (a) zonal velocity, (b) meridional velocity, (c) squared shear of horizontal velocity, (d) temperature, (e) salinity, (f) squared buoyancy frequency.

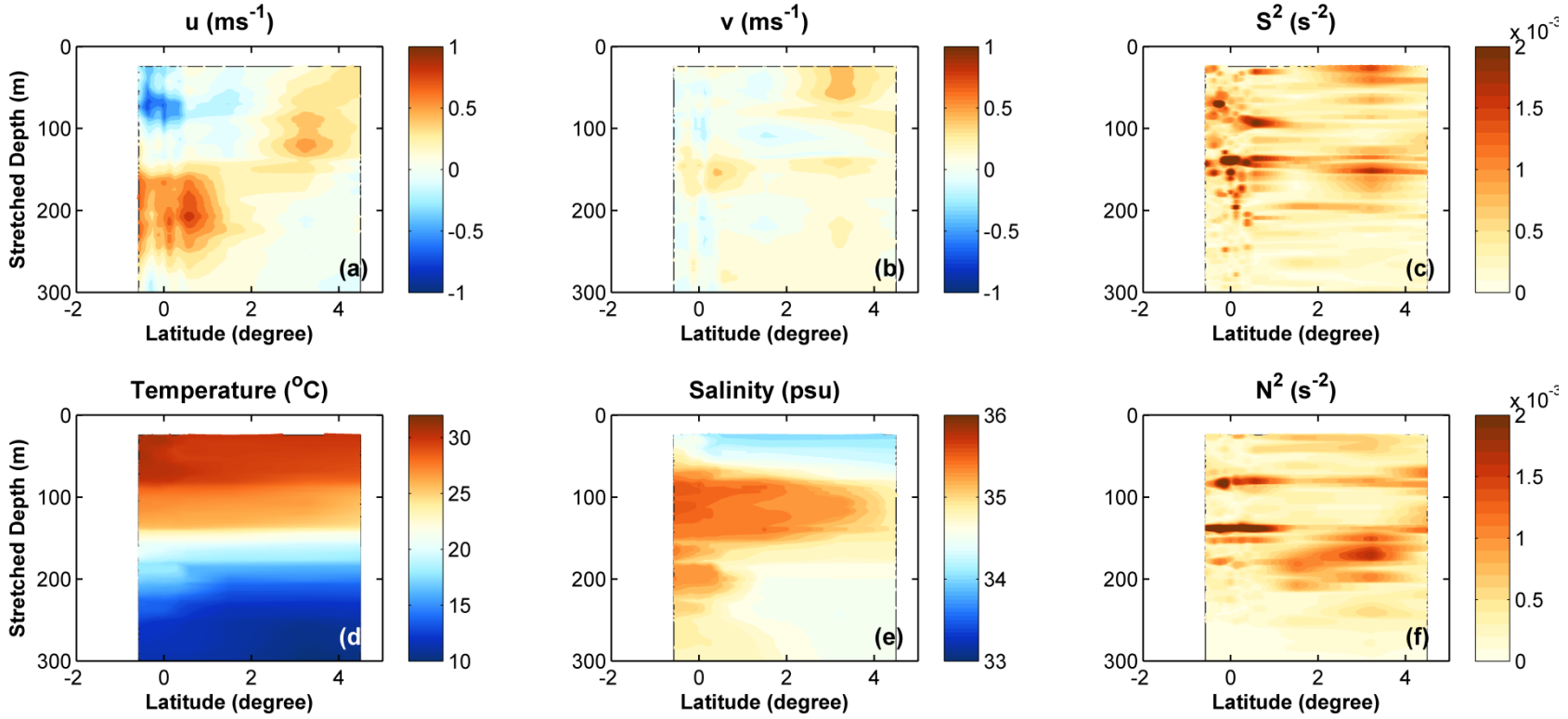

Figure 4. Section 2 (a) zonal velocity, (b) meridional velocity, (c) squared shear of horizontal velocity, (d) temperature, (e) salinity, (f) squared buoyancy frequency

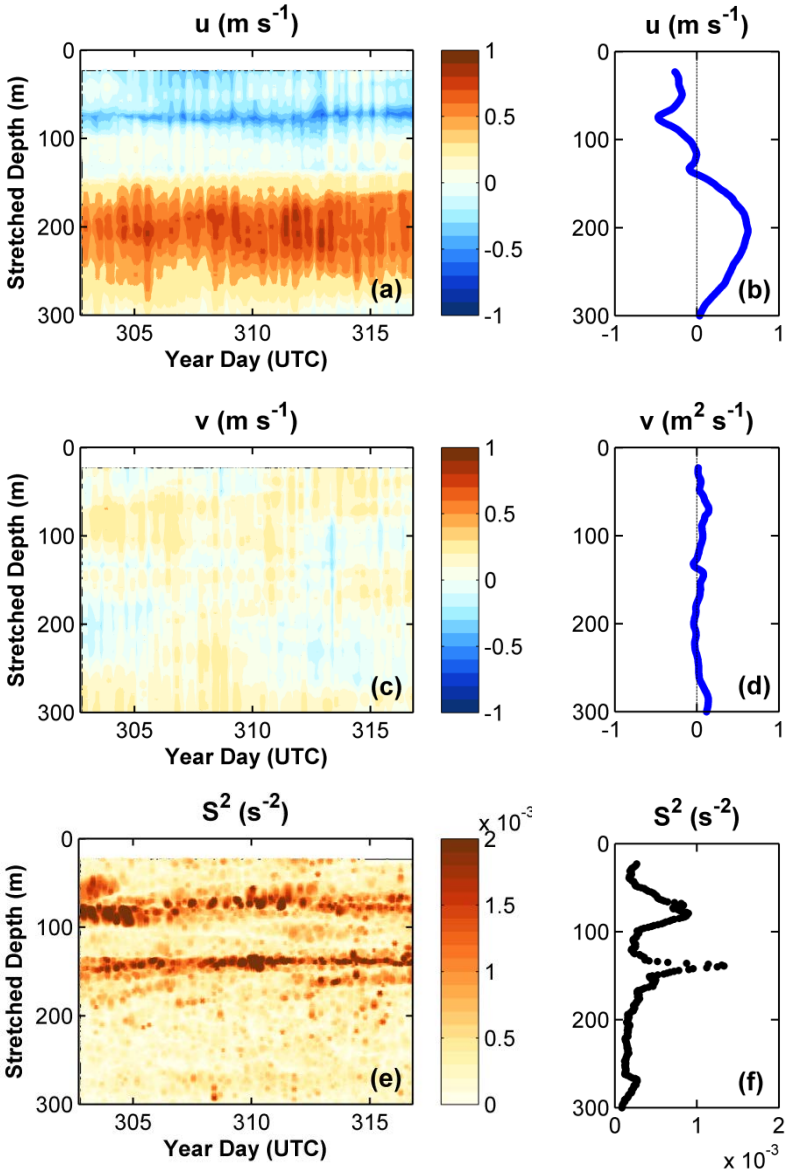

Figure 5. Time series of (a) zonal velocity, (c) meridional velocity, (e) squared shear of hosizontal velocity. Mean profiles of (b) zonal velocity, (d) meridional velocity, (f) squared shear of horizontal velocity.

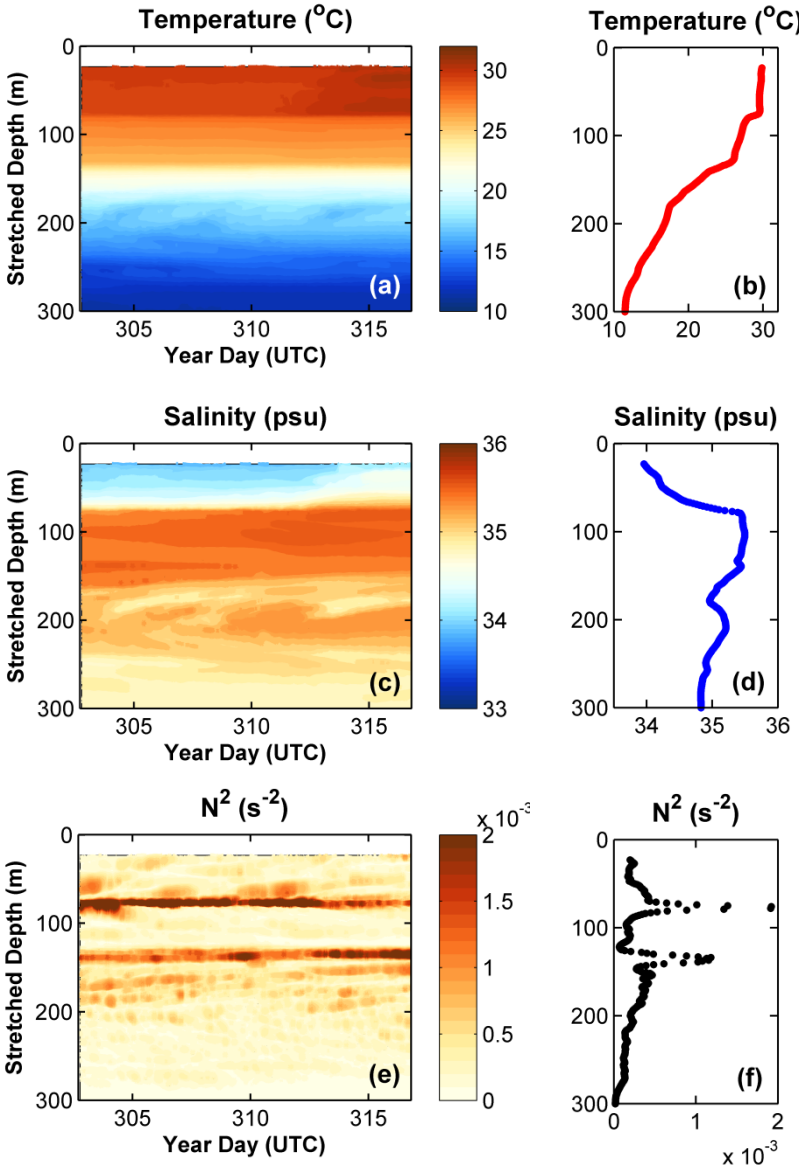

Figure 6. Time series of (a) temperature, (c) salinity, (e) squared buoyancy frequency. Mean profiles of (b) temperature, (d) salinity, (f) squared buoyancy frequency.

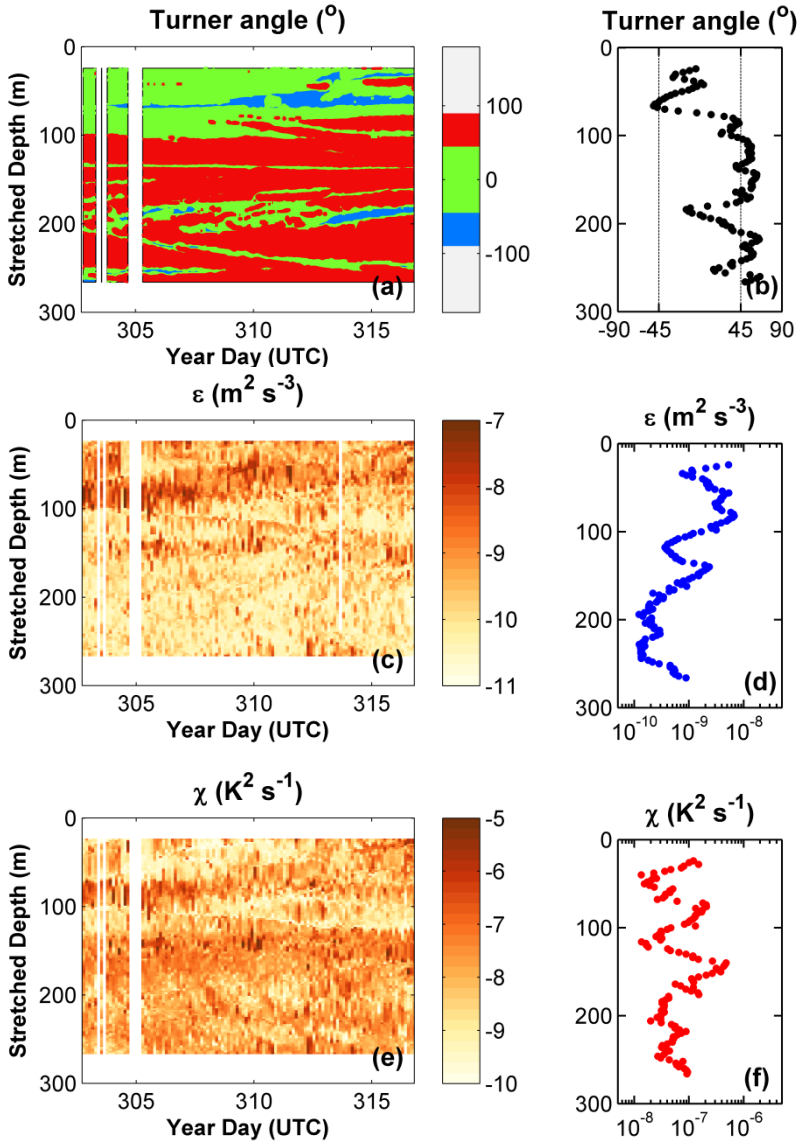

Figure 7. Time series of (a) Turner angle, (c) the dissipation rate of turbulent kinetic energy (ε), (e) the rate of loss of temperature variance (χ). Mean profiles of (b) Turner angle, (d) ε, (f) χ

2. Vertical Flux

Figure 8a - 8b shows *Re* and *Tu* to determine turbulent and double diffusive regimes based on 14-day averaged data. *Re* is less than 20 in almost whole water column except 80 – 100 m and above 30 m. Especially, below 100 m, *Re* is very small indicating turbulence is not active enough to break stratification. The profile of *Tu* is characterized by two distinct layers; no double diffusion above 100 m except at 70 m, and salt fingering below 100 m except 180 – 200 m and 250 m. We divide the averaged condition into 4 regimes based on *Re* and *Tu*; none, turbulence, non-turbulent double diffusion, and turbulent double diffusion. The dominant condition in this observation was non-turbulent double diffusive regime.

Mean profile of Γ^{obs} (equation 24) agrees well with the regimes (Figure 8c). In entirely salt fingering regime, its range is 1 – 3, similar to previous studies [*Kantha and Clayson*, 2000]. The value of in turbulent case is close to 0.2 but slightly large. This can be caused by indirect method that ignores the available potential energy making the turbulent kinetic energy dissipate [*Moum*, 1996]. Some very big Γ^{obs} are found in the diffusive convection regime because this cool and fresh water intrusion(Figure 8b, 8d) makes small temperature gradient at its core that is inversely proportional to the square root of Γ^{obs} (equation 24).

The heat and salt flux enhancement factors (equation 26 and 27) show the relative importance of effects of turbulence and double diffusion on total flux – larger the factors larger the effect of double diffusion (Figures 8e, 8f). The dominance of turbulent flux on total flux is only obvious at around 80 m. In contrasts, vertical heat flux due to salt fingering is dominant in non-turbulent salt fingering regime, about 10 times greater than that in the turbulent layer. Much larger heat enhancement factors in the diffusive convection region are due to very large Γ^{obs}, since heat enhancement factors is the

ratio of Γ^{obs} and Γ^{turb}. Vertical flux of salt is calculated only in non-turbulent double diffusive layers using the buoyancy flux ratio (γ), since we focus on double diffusive flux. Salt flux enhancement factors are almost 100 suggesting that salt fingers transport salt efficiently.

Total heat flux (equation 21) and double diffusive salt flux (equation 12) are shown in Figure 9a – 9b. Below 80 m, both have similar magnitude about 10^{-6} – 10^{-7} K m s^{-1} (psu m s^{-1}) and downward due to the dominance of the salt fingering. Largest heat flux near 70 m arises from relatively large χ compared with temperature gradient in diffusive convection regime (equation 21). This could be possible when thin interface is not captured in 2 m interval CTD profiles.

Temperature and salinity are important water properties that affect thermodynamic characteristics of seawater, including density. Since the vertical flux of temperature and salinity leads to variation of density profile, the stability of water column would be affected. In Figure 9c, density flux (equation 13) is downward due to double diffusion. In salt fingering regime, salt flux leads to downward density flux of about 10^{-7} – 10^{-8} kg m^{-2} s^{-1}.). This result suggests possibility of density flux cycle. When turbulent mixing in thermocline is suppressed possibility by salinity inducing strong stratification, downward density flux due to double diffusion allows the increase in stratification. For the turbulent dominant case like the case during the La Niña period [*Richards et al.*, 2012], positive turbulent density flux occupies whole depth range from surface to thermocline and decreases the stratification.

As we mentioned above, the observed layering experienced temporal changes alternating different regimes of diffusive convection, salt finger, and turbulence. Hence, record-length averaged data may not represent the characteristics of the layers. Figures 10 – 11 show the same vertical profiles including vertical flux, but now for three equally-divided different parts from the beginning to the end of the observation. The

main differences occur above 100 m; diffusive convection and turbulence regimes are clearly distinguished (Figure 10a – 10b). Turbulent layers with $Re > 20$ mainly occurred in the upper 120 m with peaks at different depth levels. We can obtain vertical flux of salt and density due to diffusive convection in much wider depth range as compared to the flux due to diffusive convection calculated from the record-length mean data, and the maximum magnitudes (Figure 11b-11c) are slight larger than that around 70 m in Figure 9b – 9c. Above 100 m and near 190 m, the effect of small temperature gradient on increasing Γ^{obs} and the heat flux enhancement factors becomes much clearer (Figure 10c – 10d). When temperature gradients are near zero or small negative value by periodic behaviors of interleaving layers, the profiles of Γ^{obs} have sharp peaks.

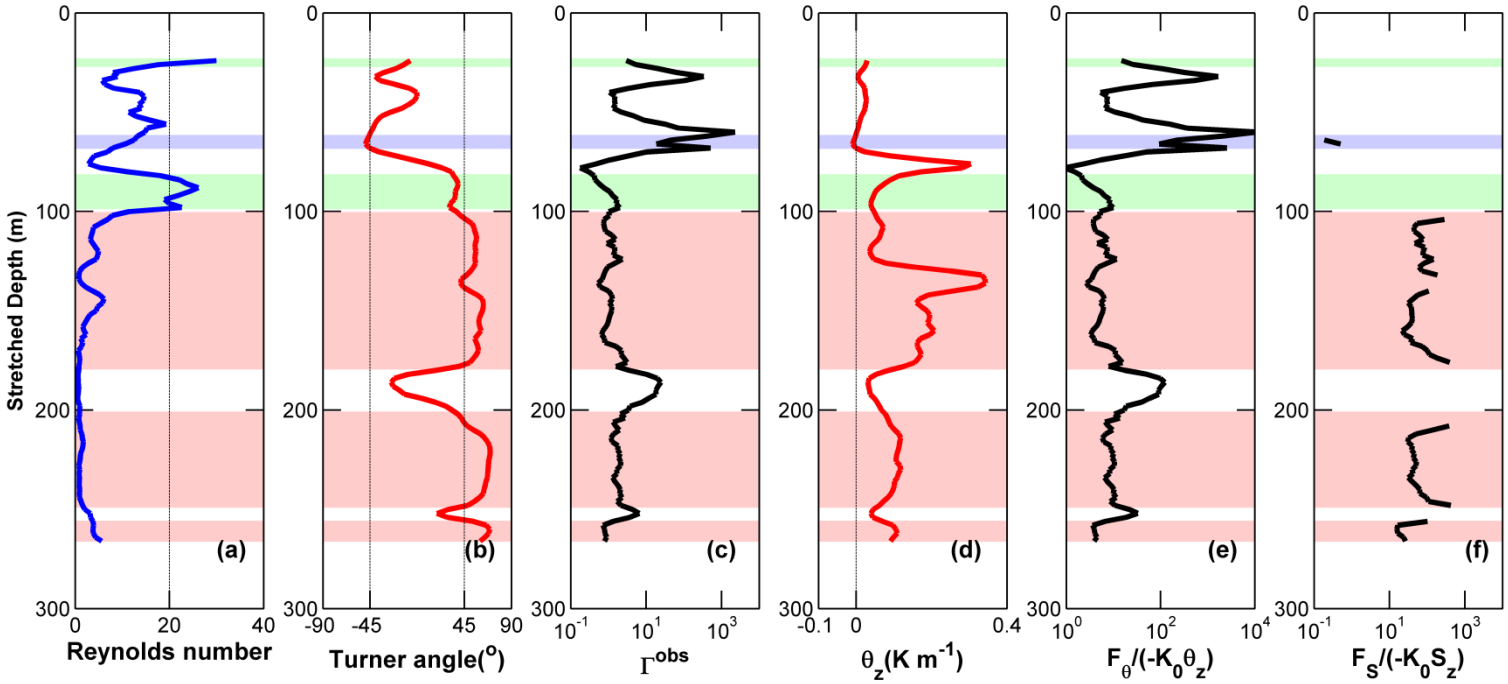

Figure 8. Vertical profiles of (a) Reynolds number, (b) Turner angle, (c) observed mixing efficiency, (d) temperature gradient, (e) het flux enhancement factors, and (f) salt flux enhancement factors [*Mcdougall and Ruddick*, 1992]. The shading display 3 regimes; light green for turbulence, light red for non-turbulent salt fingering, and light blue for non-turbulent diffusive convection. All properties are calculated from the record-length mean values of temperature and salinity.

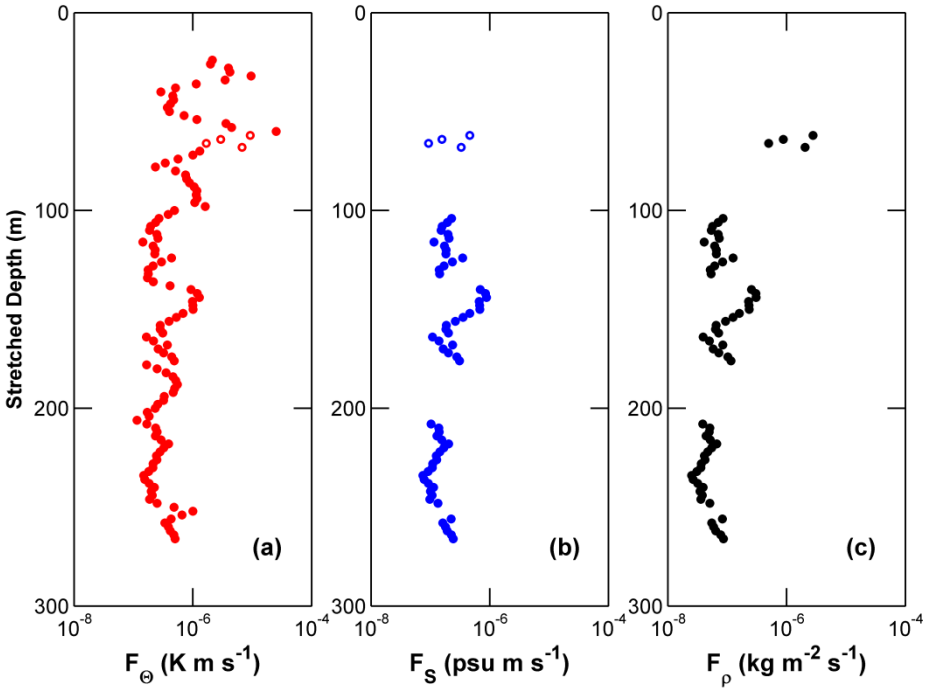

Figure 9. Vertical flux profiles of (a) heat, (b) salt, (c) density. ○ is upward and ● is downward.

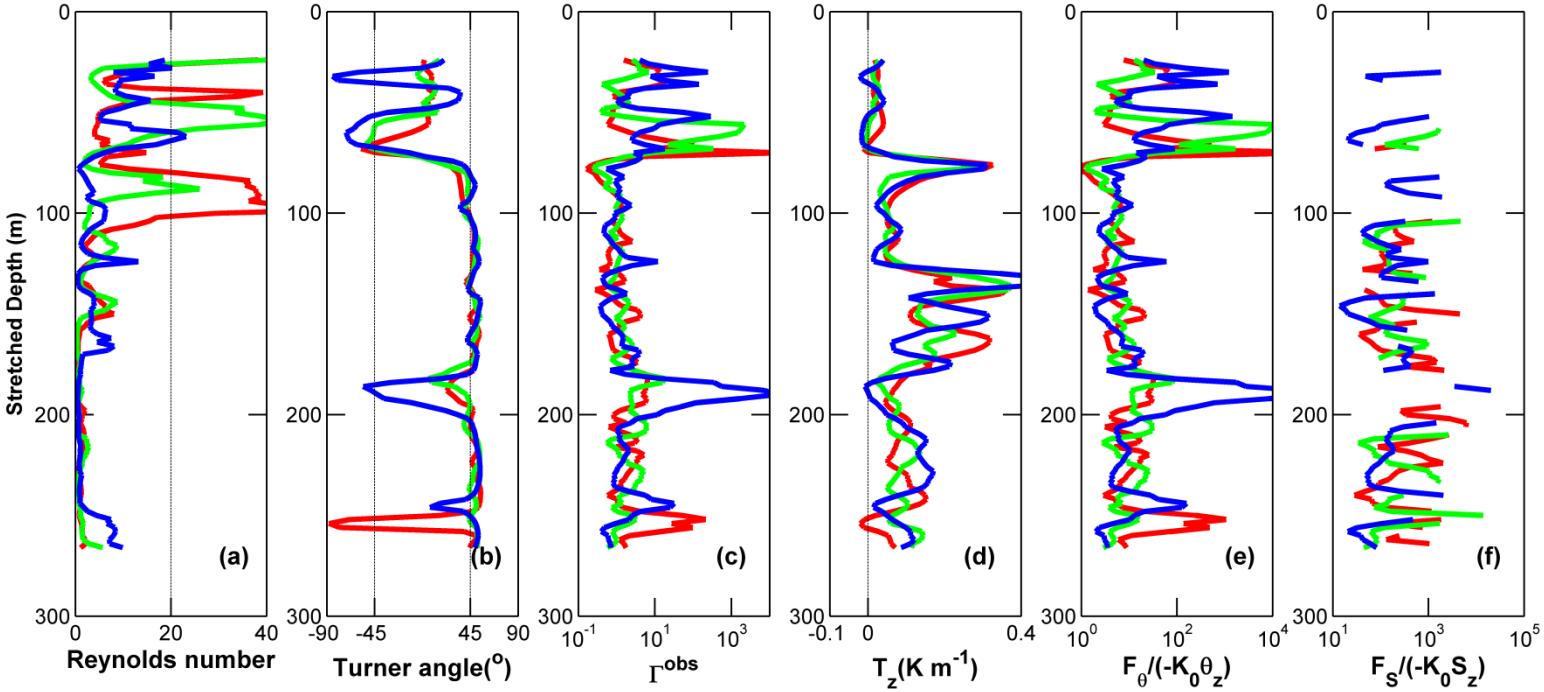

Figure 10. The same as Figure 8, but now in each of equally-divided three different parts, the red color for the first part and the blue color for the last part

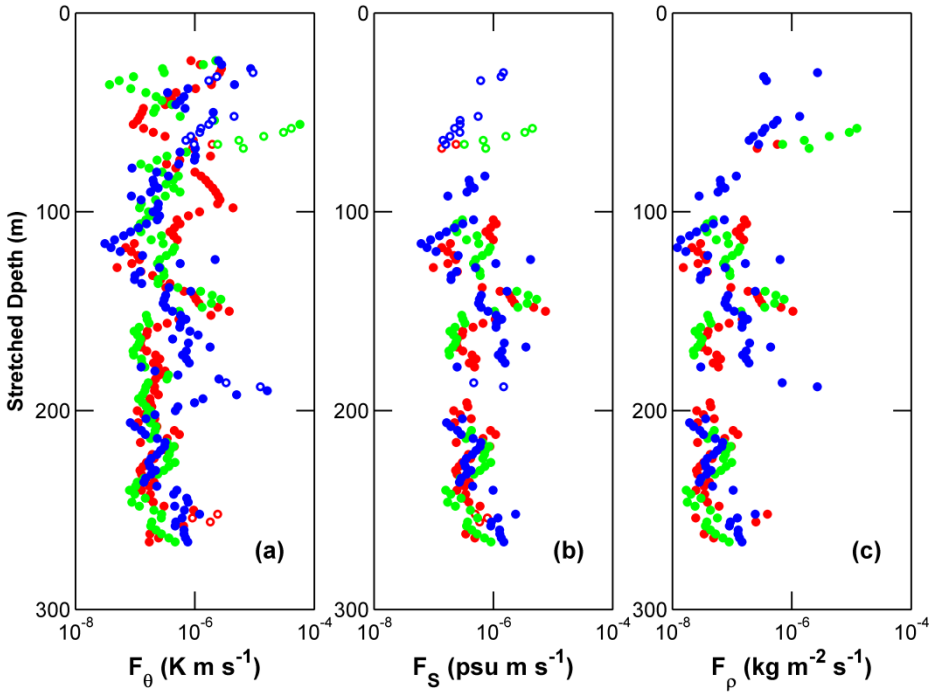

Figure 11. The same as Figure 9, but now in each of equally-divided three different parts, the red color for the first part and the blue color for the last part

3. Vertical Diffusivity

Vertical diffusivities of heat, salt, and density computed from above vertical flux are shown in Figure 12. Above 80 m, temperature diffusivity is over 10^{-3} m^2 s^{-1} but becomes reduced to be about 10^{-5} – 10^{-6} m^2 s^{-1} in thermocline region. In contrast, salinity diffusivity changes little in the vertical by about 10^{-4} – 10^{-6} m^2 s^{-1}. Density diffusivity calculated from the vertical density flux due to double diffusion is mostly downward. This result is in good agreement with theory; vertical density transport due to double diffusion is in the direction of increasing density, resulting in an increase in vertical density gradient [*Thorpe*, 2005]. Vertical diffusivities calculated in three divided periods are much noisy, but have similar patterns with those calculated from the whole data (Figure 13). The magnitude of density diffusivity of about 10^{-5} – 10^{-6} m^2 s^{-1}, is comparable or even larger than diffusivities from previous estimates based on micro-scale measurements. In tropical ocean, turbulent vertical diffusivity has similar magnitude with our results when ε is an order of 10^{-8} – 10^{-9} m^2 s^{-3} [*Gregg et al.*, 1985; *Moum et al.*, 1989; *Richard et al.*, 2012]. In conclusion, vertical density flux and associated vertical density diffusivity due to double diffusion cannot be ignored under weak turbulence condition.

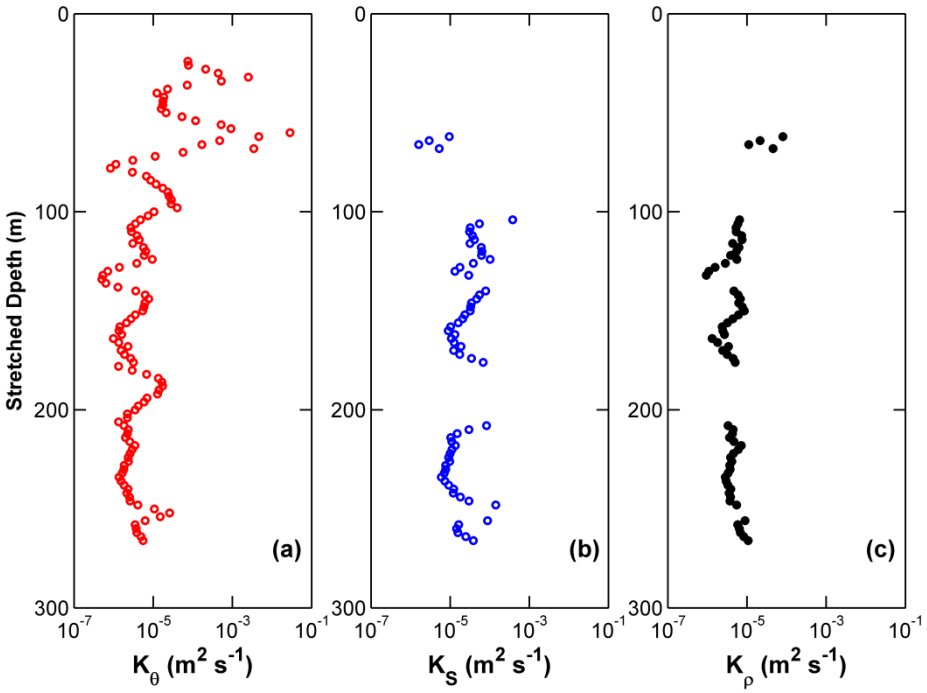

Figure 12. Vertical diffusivity profiles of (a) heat, (b) salt, (c) density. ○ is positive and ● is negative.

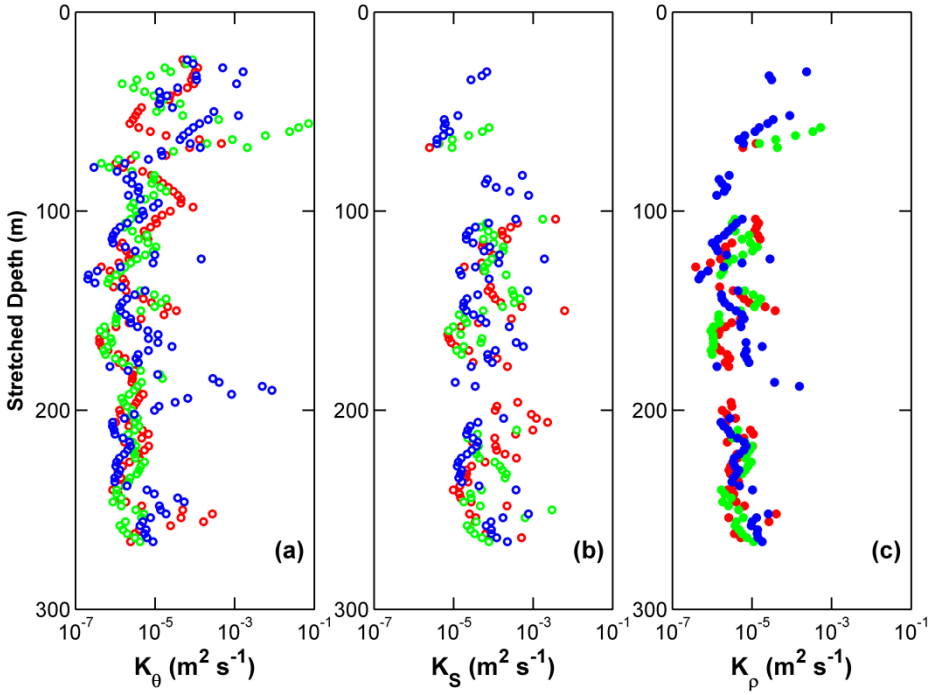

Figure 13. The same as Figure 12, but now in each of equally-divided three different parts, the red color for the first part and the blue color for the last part

Chapter 4. Conclusions

This study analyzes the effect of double diffusion and turbulence on ocean state in weak turbulence condition. We follow the method from *McDougall and Ruddick* [1992] to calculate vertical diffusivity and flux of heat, salt, and density. The upper layer from 30-270 m is divided into four regions; none, turbulence, non-turbulent double diffusion, and turbulent double diffusion based on the Reynolds number and Turner angle calculated from the observed properties. Although the observation period belongs to neither El Niño nor La Niña condition, the characteristics of ocean state and the vertical flux estimated in this study suggest three conclusions. First, the weakening of turbulence in thermocline can be caused by the strengthening of stratification due to the capping of surface warm and fresh water. This provides a clue to parameterize diffusivity in model like *Sasaki et al.* [2013]; stratification-dependent background diffusivity improves simulating the amplitude and frequency of ENSO. Second, the direction of density flux is reversed in thermocline depending on the turbulent state. The buoyancy flux caused by double diffusion is opposite to that by turbulence. The last thing is that vertical density diffusivity due to double diffusion has comparable value to that due to turbulence in strongly turbulent tropical thermocline. Considering all these factors, Buoyancy flux in the western equatorial Pacific may be reversed by propagation of fresher warm pool, but the magnitude remains in similar level. It should be emphasized that turbulence-base estimates would significantly underestimate vertical flux and diffusivity under weak turbulence condition, and double diffusive flux should be taken into consideration. More research is needed to understanding the influence of changing in the direction of density flux.

Reference

Batchelor, G. K. (1959), Small-scale variation of convected quantities like temperature in turbulent fluid Part 1. General discussion and the case of small conductivity, J. Fluid Mech., 5, 113-133, doi:10.1017/S002211205900009X

Gregg, M. C. (1988), Mixing in the thermohaline staircase east of Barbados. Small Scale Turbulence and Mixing in the Ocean, J. C. J. Nihoul and B. M. Jamart, Eds., Elsevier Oceanography Series, Vol. 46, 453–470..

Gregg, M. C., H. Peters, J. C. Wesson, N. S. Oakey, and T. J. Shay (1985), Intensive measurements of turbulence and shear in the equatorial undercurrent, Nature, 318(6042), 140-144, doi:10.1038/318140a0.

Inoue, R., H. Yamazaki, F. Wolk, T. Kono, and J. Yoshida (2007), An Estimation of Buoyancy Flux for a Mixture of Turbulence and Double Diffusion. J. Phys. Oceanogr., 37, 611–624, doi:10.1175/JPO2996.1.

Itsweire, E. C., J. R. Koseff, D. A. Briggs, and J. H. Ferziger (1993), Turbulence in Stratified Shear Flows: Implications for Interpreting Shear-induced Mixing in the Ocean, J. Phys. Oceanogr., 23, 1508–1522, doi:10.1175/1520-0485(1993)023<1508:TISSFI>2.0.CO;2.

Johnson, G. C., B. M. Sloyan, W. S. Kessler, and K. E. McTaggart (2002), Direct measurements of upper ocean currents and water properties across the tropical Pacific during the 1990s, Prog. Oceanogr., 52, 31–-61, doi:10.1016/S0079-6611(02)00021-6.

Kantha, L. H., and C. A. Clayson (2000), Small scale processes in geophysical fluid flows (Vol. 67), Academic Press.

Kelley, D. E. (1990), Flux through diffusive staircases: A new formulation, J. Geophys. Res., 95(C3), 3365–3371, doi:10.1029/JC095iC03p03365.

Kunze, E. (1987), Limits on growing, finite-length salt fingers: A Richardson number constraint. Journal of Marine Research, 45(3), 533-556, doi:10.1357/002224087788326885.

Lien, R. C., D. R. Caldwell, M. C. Gregg,, and J. N. Moum (1995), Turbulence variability at the equator in the central Pacific at the beginning of the 1991–1993 El Nino. Journal of Geophysical Research: Oceans (1978–2012), 100(C4), 6881-6898, doi: 10.1029/94JC03312.

Linden P. F. (1971), Salt fingers in the presence of grid-generated turbulence. J. Fluid Mech., 49, pp 611624, doi:10.1017/S0022112071002283.

Maes, C., K. Ando, T. Delcroix, W. S. Kessler, M. J. McPhaden, and D. Roemmich (2006), Observed correlation of surface salinity, temperature and barrier layer at the eastern edge of the western Pacific warm pool, Geophys. Res. Lett., 33, L06601, doi:10.1029/2005GL024772.

McDougall, T. J. and B. R. Ruddick (1992), The use of ocean microstructure to quantify both turbulent mixing and salt-fingering, Deep Sea Res., 39, 11-12, 1931–1952, doi:10.1016/0198-0149(92)90006-F.

Meehl, G. A., P. R. Gent, J. M. Arblaster, B. L. Otto-Bliesner, E. C. Brady, and A. Craig (2001), Factors that affect the amplitude of El Niño in global coupled climate models, Climate Dynamics, 17(7), 515-526, doi:10.1007/PL00007929.

Moum, J. N. (1996), Efficiency of mixing in the main thermocline, J. Geophys. Res., 101(C5), 12057–12069, doi:10.1029/96JC00508.

Moum, J. N. and D. R. Caldwell (1985), Local influences on shear-flow turbulence in

the equatorial ocean, Science, 230(4723), 315-316, doi:10.1126/science.230.4723.315.

Moum, J. N., D. R. Caldwell, and C. A. Paulson (1989), Mixing in the equatorial surface layer and thermocline. Journal of Geophysical Research: Oceans (1978–2012), 94(C2), 2005-2022, doi:10.1029/JC094iC02p02005

Moum, J. N., R. C. Lien, A. Perlin, J. D. Nash, M. C. Gregg, and P. J. Wiles (2009), Sea surface cooling at the equator by subsurface mixing in tropical instability waves, Nature Geoscience, 2(11), 761-765, doi:10.1038/NGEO657.

Nasmyth, P. W. (1973), Turbulence and microstructure in the upper ocean, Mem. Soc. Roy. Sci. Liege, Ser, 6(4), 47-56.

Osborn, T. R. (1980), Estimates of the Local Rate of Vertical Diffusion from Dissipation Measurements, J. Phys. Oceanogr., 10, 83–89, doi:10.1175/1520-0485(1980)010<0083:EOTLRO>2.0.CO;2.

Padman, L. and T. M. Dillon (1987), Vertical heat flux through the Beaufort Sea thermohaline staircase, J. Geophys. Res., 92, 10 799–10 806, doi:10.1029/JC092iC10p10799.

Richards, K. J. and H. Banks (2002), Characteristics of interleaving in the western equatorial Pacific, J. Geophys. Res., 107(C12), 3231, doi:10.1029/2001JC000971.

Richards, K. J. and R. T. Pollard (1991), Structure of the upper ocean in the western equatorial Pacific, Nature, 350, 48– 50, doi:10.1038/350048a0.

Richards, K. J., Y. Kashino, A. Natarov, and E. Firing (2012), Mixing in the western equatorial Pacific and its modulation by ENSO, Geophys. Res. Lett., 39, L02604, doi:10.1029/2011GL050439.

Ruddick, B. and K. Richards (2003), Oceanic thermohaline intrusions: observations. Progress in Oceanogr., 56, (3-4), 499-527, doi:10.1016/S0079-6611(03)00028-4.

Sasaki, W., K. J. Richards, and J.-J. Luo (2013), Impact of vertical mixing induced by small vertical scale structures above and within the equatorial thermocline on the tropical Pacific in a CGCM, Climate Dynamics, 41, 2, 443-453, doi:10.1007/s00382-012-1593-8.

Schmitt, R. W., J. R. Ledwell, E. T. Montgomery, K. L. Polzin, and, J. M. Toole (2005), Enhanced diapycnal mixing by salt fingers in the thermocline of the tropical Atlantic. Science, 308(5722), 685-688, doi:10.1126/science.1108678.

St. Laurent, L. and R. W. Schmitt (1999), The Contribution of Salt Fingers to Vertical Mixing in the North Atlantic Tracer Release Experiment, J. Phys. Oceanogr., 29, 1404–1424, doi:10.1175/1520-0485(1999)029<1404:TCOSFT>2.0.CO;2.

Thorpe, S. A. (2005), The turbulent ocean, Cambridge University Press., New York.

Tomczak, M., and Godfrey, J. S. (2003), Regional oceanography: an introduction, Daya Books.

Wolk, F., H. Yamazaki, L. Seuront, and R. G. Lueck (2002), A new free-fall profiler for measuring biophysical microstructure, J. Atmos. Oceanic Technol., 19(5), 780-793, doi:10.1175/1520-0426(2002)019<0780:ANFFPF>2.0.CO;2.

국문 초록

적도 서태평양에서 이중 확산에 의한 수직 혼합 산출

이 초 롱
지구환경과학부
서울대학교 대학원

본 연구는 2012년에 0 ° N, 156 ° E에서 관측한 14일 간의 시계열 자료를 이용하여 난류가 약한 시기에 이중확산이 수온약층(약 20 m에서 300 m보다 깊은 수심까지)의 수직혼합에 미치는 영향을 알아보고자 하였다. 이 관측에서는 미규모 관측장비를 이용하여 온도 소산율과 난류 운동 에너지 소산률을 직접 계산하였다. 관측 시기는 엘니뇨나 라니냐가 일어나지 않았던 시기임에도 불구하고, 엘니뇨 시기와 유사하게 온난해수역의 서쪽 확장으로 야기된 강한 성층이 표층과 수온약층의 상호작용을 억제하여 수온약층에서 난류가 약하였다. 온도와 염분, 밀도의 수직확산계수와 속은 *McDougall and Ruddick* [1992]의 방법을 따랐다. 난류와 이중확산이 일어나는 지역을 나누는 기준은 터너 각(Turner angle)과 레이놀즈 수(Reynolds number)을 시용하여 수직혼합이 일어나지 않는 구간, 난류 구간, 이중확산 구간, 난류와 이중확산이 동시에 존재하는 구간으로 나누었다. 연구 결과에 따르면 수온약층의 대부분에서 난류가 약하여 이중확산이 지배적이었다. 이중확산에 의한 수직 열속과 수직 염속은 난류보다 10-100배 정도 큰 10^{-6} - 10^{-7} K m s^{-1}, 10^{-5} - 10^{-6} psu m s^{-1}의 값을 가졌다. 이중확산으로 인한 수직 밀도속은 성층을 더 강화시키는 하향으로 10^{-7} kg m^{-2} s^{-1} 정도로 나타난다. 이중확산에 의한 밀도의 수직확산계수는 10^{-5} - 10^{-6} m^2 s^{-1}로, 적도에서 난류에너지 소산율이 10^{-8} - 10^{-9} m^2 s^{-3}일 때의 난류에 의한 밀도의 수직확산계수의 값과 맞먹는다. 본 연구에서 난류가 약할 때, 적도 서태평양의 수직 밀도속에 이중확산이 큰 기여를 하는 것을 알 수 있었다. 따라서 난류에 의해서만 수직 속을 구한다면 실제보다 작게 추정될 가능성이 높다.

주요어: 난류, 이중확산, 수직혼합, 적도 서태평양
학번: 2012-23080